PIV Measurements of the Wake of a Tandem-Rotor Helicopter in Proximity to a Ship

Alan J. Wadcock
Aerospace Computing, Inc
Moffett Field, CA
awadcock@mail.arc.nasa.gov

Gloria K. Yamauchi
NASA Ames Research Center
Moffett Field, CA
yamauchi@mail.arc.nasa.gov

James T. Heineck
NASA Ames Research Center
Moffett Field, CA
jheineck@mail.arc.nasa.gov

Mark J. Silva
Naval Air Warfare Center
Patuxent River, MD
mark.silva@navy.mil

Kurtis R. Long
Naval Air Warfare Center
Patuxent River, MD
klong@mail.arc.nasa.gov

Abstract

The aerodynamic interaction between a tandem-rotor helicopter and an amphibious assault ship is described. The investigation was jointly sponsored by NASA and the U.S. Navy, using 1/48th-scale helicopter and ship models. The test was conducted in the Army 7- by 10-Ft Wind Tunnel at NASA Ames Research Center. Particle Image Velocimetry (PIV) was used to acquire 3-component velocity field measurements of the ship air-wake and the combined wake of the tandem-rotor helicopter and ship. Ship-alone air-wake measurements are presented for yaw angles of 0, 5, 10 and 15 degrees, for a wind speed of 22.5 ft/sec at one aircraft landing spot of primary interest. The combined wake of the tandem-rotor helicopter and the ship air-wake are described in considerable detail at the same landing spot for both zero and fifteen degrees yaw angle. Variation of the combined wake with position of the upwind aircraft is described in detail. These measurements provide guidance in planning shipboard operations of rotorcraft.

Notation

A	aircraft total rotor disk area ($2\pi R^2$)
b	tilt-rotor wingspan
c	blade chord
C_T	aircraft thrust coefficient, $T/(\rho(\Omega R)^2 A)$
D	rotor diameter
DW	downwind
M_{tip}	blade tip Mach number, ΩR/(sound speed)
N	number of blades
R	rotor radius
T	aircraft total thrust
UW	upwind
WHOD	wheel height over deck
μ	advance ratio, tunnel speed/(ΩR)
Ω	rotor rotational speed
ρ	air density
σ	rotor solidity, $Nc/(\pi R)$

Presented at the AHS 4th Decennial Specialist's Conference on Aeromechanics, San Francisco, CA, January 21-23, 2004.

Introduction

The difficulties in making accurate full-scale shipboard-operations measurements are many. Variability of the wind in both magnitude and direction and the difficulty of measuring the wind velocity free from any influence of the ship itself are a major concern. Waiting for quiescent atmospheric conditions and then sailing at a known speed can eliminate this difficulty. Unfortunately, this approach is economically unfeasible. In addition to the variability of the *mean* velocity of the wind, full-scale testing must cope with the presence of an atmospheric boundary layer of variable thickness, plus gusts or turbulence. Sea trials must also cope with motion of the flight deck caused by wave motion (surge, sway and heave; roll, pitch and yaw). The wind tunnel is the ideal environment for such studies because the wind tunnel provides accurate control over test conditions. A comprehensive wind tunnel test is a cost-effective approach that allows a flight test program to concentrate full-scale shipboard operations on test conditions of greatest concern.

The Army/NASA Rotorcraft Division at NASA Ames Research Center and the U.S. Navy recently conducted a study to investigate the aerodynamics of shipboard operation of rotorcraft. The present study was motivated by the uncommanded roll

experienced by a V-22 parked on deck with rotors turning while a CH-46 approached the deck for landing (Ref. 1). Measurements were divided between two wind tunnel entries. The first wind tunnel entry measured forces and moments on the on-deck tilt-rotor as a function of the upwind tandem-rotor helicopter position, and documented the ship air-wake and the combined wake of the helicopter and ship. This work was completed in April 2002. Reference 2 provides an overview of these measurements while Reference 3 documents the experiment in detail. A second wind tunnel entry, completed in November 2003, provided similar measurements with the UW tandem-rotor helicopter replaced by either a single-main-rotor helicopter or a tilt-rotor.

The 1/48th-scale models are adequate for simulating gross aerodynamic interactions between the ship and rotorcraft since the parameters that govern the strength and position of the trailed rotor wake are rotor thrust and forward speed, not details of the rotor geometry. If key non-dimensional parameters such as rotor thrust coefficient and advance ratio can be matched between model and full-scale, the model scale data should provide a good representation of full-scale events. Previous work at Ames Research Center using small (approximately 1/40th-scale) tilt-rotor models have proven the viability of using models of this size for aerodynamic investigations (References 4 and 5). Reference 6 provides a detailed description of the design and construction of both the ship and various 1/48th-scale helicopter models. References 7 and 8 describe the use of similar tilt-rotor models to study the aerodynamic interaction between tilt-rotor aircraft in formation flight.

This paper presents measurements of ship-alone air-wake plus the combined wake of the ship and upwind tandem-rotor helicopter for selected conditions of interest. Particle Image Velocimetry (PIV) was used to acquire 3-component velocity fields in several cross-flow planes along the ship deck to define the ship-alone air-wake for various combinations of ship yaw and wind speed. The paper describes the ship and aircraft models and the PIV set-up. PIV measurements of the ship alone air-wake are presented for yaw angles of 0, 5, 10 and 15 degrees. PIV measurements of the combined helicopter plus ship air-wake are presented for yaw angles of 0 and 15 degrees only. PIV measurements described in the current paper are limited to a single streamwise station just downstream of the island.

Facility Description

The 7- by 10-Ft Wind Tunnel is a closed circuit wind tunnel operated by the U.S. Army Aeroflightdynamics Directorate at NASA Ames Research Center. The test section is 7-ft high, 10-ft wide and 15-ft long. The tunnel has a 14:1 contraction ratio providing a maximum speed of approximately 350 ft/sec. Four high-loss turbulence-reduction screens are installed in the return duct. The test section turntable is capable of yaw angles up to 360 degrees. An air exchange system allows up to 29% air exchange. Since wind speeds for this experiment ranged from 5.6 to 33.8 ft/s, the tunnel was run with 0% air exchange to eliminate atmospheric influence on the test section flow steadiness. The measurement of such low free-stream velocities necessitated the use of a 1-mbar differential pressure transducer to measure test section dynamic pressure, limiting the free stream velocity to slightly more than 40 ft/sec. A computer-controlled test-section traverse system is capable of traversing in the vertical, lateral, and streamwise directions.

Model Description

Most of the hardware for this experiment was designed and fabricated by NASA Ames. 1/48th-scale models of the ship, a single main rotor helicopter, a tandem rotor helicopter and two tilt-rotors were fabricated. Reference 6 provides details of the design methodology and construction for all the models.

Ship

Figure 1 shows the ship installed in the 7- by 10-Ft Wind Tunnel. The ship is a low-fidelity 1/48th-scale model of an LHA amphibious assault ship. Key dimensions are provided in Table 1. The ship is mounted 15 inches off-axis in the wind tunnel to accommodate the tandem-rotor helicopter simulated flight patterns to be flown off the port side of the ship. The ship is mounted to the turntable in order to provide model yaw.

The model-scale flight deck has several sets of markings known as "crow's foot" markings that duplicate full-scale markings at each landing spot. These markings provide visual cues to the pilot during shipboard rotorcraft approach, hover, descent and departure sequences. Each crow's foot marking, at full scale, consists of 2 ft-wide white stripes that extend 10 to 30 ft laterally, forward, and diagonally inwards from the landing spot center. Equivalent line width at model scale is 0.5 inches. Each crow's foot is normally associated with a set of nose-wheel and landing gear wheel spots. Numerous landing spot markings are visible in Figure 1.

Even at 1/48th-scale, the ship model is very large. From Table 1, overall deck width is 2.46 ft, length is 17.08 ft and height of deck above test section floor is 1.34 feet. Model blockage is non-negligible, but is acceptable for the 0 to 15-degree portside winds of the current study. In the immediate vicinity of the island the maximum blockage ratio is 5.76% for the ship at a

yaw angle of zero degrees. The corresponding value at 15 deg yaw becomes 5.96%.

Tandem-Rotor Helicopter

The basic geometry (rotor diameter, solidity, rotor-rotor position) of a CH-46 provides the primary dimensions for the tandem-rotor helicopter model. Characteristic dimensions of the approximate 1/48th-scale model are provided in Table 2. Figure 2(a) shows an assembly drawing of the essential component parts. The rotor transmissions are radio-controlled helicopter tail-rotor assemblies. The three-bladed hubs have counter-clockwise rotation on the forward rotor and clockwise rotation on the aft rotor (viewed from above). The model has rigid hubs with collective control only (no cyclic pitch control). Differential collective pitch can be introduced to trim pitching moment if so desired. Available motor power limited the design rpm of the model to 1/3 that of full-scale.

The full-scale CH-46 has a nose-down shaft tilt of 9.5 deg for the forward rotor and 7.0 deg for the aft rotor. Representative trimmed tip-path-plane angles, relative to free-stream, were predicted to be 2.2 deg nose-down for the forward rotor and 0.6 deg nose-up for the aft rotor for an aircraft of weight 18,500 lbs at sea level. These should be compared with tip-path-plane angles of 2.5 deg nose-down and horizontal chosen for the model-scale helicopter, the aft transmission being higher than the forward transmission. The same calculations indicated 49% & 51% thrust sharing between the forward and aft rotors for a c.g. at the mid-point between the two rotors. Differential collective pitch was used to establish the desired aircraft center of thrust in hover and then left fixed for the duration of the test.

The model was mounted on a 0.75-inch six-component Task balance to measure aircraft forces and moments. The balance block at the rear of the model is identified in Figure 2(a). Figure 2(b) shows the tandem-rotor helicopter model, plus fuselage, sting-mounted from a streamlined strut suspended beneath the tunnel traverse system. The survey apparatus is under computer control allowing the helicopter to be positioned at any desired position alongside the ship. The streamlined strut has a fixed orientation with respect to the free-stream direction. The sting, however, can be manually rotated to deliver pre-set yaw angles of the UW aircraft. This allows the UW aircraft to "fly" an approach parallel to the longitudinal axis of the ship whilst maintaining minimum aerodynamic interference from the support hardware. The aircraft pitch was fixed at zero. The aft rotor tip-path-plane was therefore horizontal.

On-deck Tilt-Rotor

The geometry of the on-deck tilt-rotor model, an approximate 1/48th-scale model of a V-22 Osprey, is detailed in Ref. 6. Characteristic dimensions are listed in Table 2. This on-deck aircraft was mounted on a fixed pedestal sting attached to the ship deck so as to position the tilt-rotor at either Landing Spot 7 (Fig. 3) or Landing Spot 8 (Fig. 4). This model was absent for the ship-alone air-wake measurements which were made with a clean deck. During the combined ship-plus-helicopter wake PIV measurements at Spot 7 (actually at the location of the rotors for an on-deck V-22 at Spot 7) this model remained mounted at Spot 8, but was non-operational. It is assumed that any upstream influence of the stationary (non-rotating) on-deck tilt-rotor on the PIV measurement plane is negligible.

PIV Installation

Figure 5 is a schematic showing the relative placement of the Laser Light Sheet (LLS) optics, PIV cameras and ship. The LLS was placed at a fixed streamwise location in the tunnel and the ship was translated streamwise thus eliminating the need for multiple camera calibrations. One disadvantage of this approach is that the LLS remains in the cross-flow plane when the ship is yawed, so that the LLS is no longer perpendicular to the longitudinal axis of the ship. This is illustrated in Figure 6 where the LLS is shown located 4.53 in downstream of the Spot 7 nose-wheel location (5.53 in downstream of Spot 7 crows foot) at the rotor location of an on-deck V-22 at that landing spot. Figure 6(a) shows the case of 0 deg yaw, whilst Figure 6(b) corresponds to 15 deg yaw. Figure 6 also indicates that as the ship is yawed, the UW aircraft maintains the same yaw angle as the ship. A very large measurement field is required to cover both ship air-wake and the wake from the helicopter flying approach patterns off the port bow. The PIV flow field is therefore centered in the test section despite the ship being mounted off-axis. The PIV flow field size is approximately 6 ft horizontal x 3 ft vertical. The nominal LLS thickness at the ship deck was 6 mm.

The laser is a Spectra Physics PIV 400 dual-oscillator Nd:Yag laser with 350 mJ/pulse at 532 nm wavelength. The LLS was folded back on itself to increase the optical path length prior to launch into the test section as illustrated in Figure 5. This reduced the required beam expansion angle in the vertical plane thereby minimizing the variation in sheet intensity from one side of the tunnel to the other. The position of the LLS was marked both on the entry window and the far wall of the test section. This provided a simple means of monitoring any motion of the LLS in the streamwise direction. High-resolution Kodak ES 4.0 2k x 2k digital cameras were used in order to provide the desired

spatial resolution (Figures 7, 8). These cameras were used in forward scatter, 30 degrees off-axis, as shown in Figures 5 and 7. This results in optimal particle visibility whilst maintaining acceptable perspective in the image. Each camera is equipped with a 50 mm f/1.4 Nikkor lens mounted on motorized rotation and translation stages to satisfy the Scheimpflug focusing condition as shown in Figure 8.

A single Corona Integrated Technologies Vicount 5000 2.2 kW Series 180 mineral oil smoke generator was used to seed the flow. Smoke was injected into the primary diffuser immediately downstream from the test section.

Software control of the camera trigger at 2 Hz ($1/6^{th}$ the laser rep rate) was used to avoid loss of data. This trigger was not synched with either the upwind rotor or the on-deck rotor. The maximum out-of-plane particle displacement was kept small (less than 25%) in comparison to the LLS thickness in order to provide a strong correlation. In-plane particle displacements were kept below 4 pixels. Once satisfactory conditions were met, 100 frames of data were acquired for each test condition. The data were processed with a 24-pixel cross-correlation window without difficulty. The corresponding spatial resolution of the measurements is 0.8 inches horizontal and 0.4 inches vertical (equivalent full-scale spatial resolutions of 3.4 ft and 1.7 ft respectively).

Test Procedure

Flow field measurements were acquired for the ship alone and for the combined configuration of ship plus upwind helicopter. Ship-alone air-wake data were acquired at multiple landing spots in a plane perpendicular to the freestream. Data were acquired for ship yaw angles between 0 and 15 degrees (yaw to starboard) and tunnel speeds from 5.6 to 33.8 ft/s as indicated in Table 3. In order to establish test conditions of interest for flow field measurements of the combined wake of the ship plus upwind helicopter, the following procedure was followed. Force and moment data of both aircraft were first acquired for various combinations of UW helicopter position, wind tunnel speed and ship yaw angle for a given location of the on-deck tilt-rotor. The on-deck tilt-rotor was first trimmed to an initial low thrust level and zero rolling moment under the influence of the ship-alone air-wake with the non-rotating UW helicopter positioned up and away. On-deck rolling moment measurements therefore indicate the change in rolling moment due to the UW aircraft from the baseline rolling moment due to the ship-alone air-wake. The UW aircraft was then set at the desired thrust (C_T=0.0048 in this case) and traversed in a pre-programmed grid in the horizontal plane at a fixed height above the ship deck while the on-deck tilt-rotor forces and moment were allowed to vary. Figure 9 shows the geometry used to identify the UW helicopter position. The UW helicopter was re-trimmed to the target C_T of 0.0048 at each grid point before force and moment data from both aircraft were acquired. Using this procedure, the forces and moments of the on-deck tilt-rotor were mapped as a function of the upwind helicopter position for a given tunnel speed and ship yaw angle. Conditions resulting in peak roll moments on the on-deck tilt-rotor were then identified and used to establish test conditions of interest for follow-on PIV measurements.

Test Conditions

Ship-alone air-wake data were acquired for the conditions listed in Table 3. Complete documentation of the ship-alone air-wake can be found in Ref. 3. Landing Spots 5 and 6 were not documented due to blockage of the LLS by the island. Reynolds Number effects are assumed to be minimal due to the sharp edges of the deck and superstructure that fix the separation location. The position of the LLS was chosen to coincide with the center of the rotor disk for an on-deck tilt-rotor at each landing spot. The streamwise nose-wheel to rotor hub distance for the V-22 is 217.5 in = 18.125 ft at full-scale. At model scale this distance becomes 4.53 in. The LLS was therefore positioned 4.53 in downstream of the nose-wheel marker at each landing spot. Note that the nose-wheel marker is 4 ft downstream from the center of the crows foot (1 inch at model scale). The current paper presents ship-alone air-wake measurements for yaw angles of 0, 5, 10 and 15 degrees, for a wind speed of 22.5 ft/sec at Landing Spot 7 only. For efficiency, the position of the LLS in the tunnel was not changed as the ship was yawed. The result is a LLS that is no longer perpendicular to the longitudinal axis of the ship for non-zero yaw angles, and whose position has moved slightly with respect to a fixed location on the ship deck (recall Figure 6).

Desire to match advance ratio for the helicopter model operated at 1/3 of full-scale tip speed dictated the low-speed matrix used for testing. The test matrix was composed of free-stream velocities from 14.1 to 25.3 ft/sec (equivalent full-scale wind speeds of 25 to 45 knots). Combined ship plus tandem-rotor helicopter wake measurements presented in the current paper concentrate on a single wind speed of 19.7 ft/sec (equivalent full-scale wind speed of 35 knots). The current paper provides data for ship (and helicopter) yaw angles of 0 and 15 degrees at Landing Spot 7. The LLS was again located 4.53 in downstream of the nose-wheel marker at Spot 7. The LLS position in the wind tunnel was not adjusted for motion along the deck caused by ship yaw. Combined ship plus tandem-rotor helicopter wake measurements presented in this paper

were made at Spot 7 with the configuration shown in Figure 4, with an unpowered on-deck tilt-rotor model at Spot 8. The goal was to simulate a clear deck for the PIV measurements without actually removing the on-deck aircraft. It is assumed that any upstream influence from this non-rotating tilt-rotor is insignificant at the plane of the PIV measurements.

Results and Discussion

All PIV data presented in this paper are limited to Spot 7 in a plane perpendicular to the free stream (independent of ship yaw). All vector flowfield measurements described in this paper refer to the mean flowfield defined by the ensemble average of 100 frames of data. A frame refers to a single instantaneous velocity field. Individual mean velocity components have been normalized with the appropriate free stream wind speed. No corrections for blockage have been made. In all cases, PIV flowfields are presented viewed looking upstream.

Ship alone air-wake

The ship-alone air-wake measurements were made with a clean deck. Figure 10 presents ship-alone air-wake measurements for yaw angles of 0, 5, 10 and 15 deg for a wind speed of 22.5 ft/sec at Landing Spot 7. The position of the LLS in the tunnel was not changed as the ship was yawed.

Figure 10 shows the mean in-plane velocity components (normalized with the wind speed) in the form of vectors and the mean out-of-plane velocity component in the form of a color-coded contour plot. The length of each arrow is proportional to the local speed. Only 25% of the in-plane velocity vectors are shown for clarity (every second vector in both vertical and lateral directions). Figure 10(a) shows flowfield measurements at Landing Spot 7 for 0 deg yaw. The island profile and the deck outline are included in the figure. Sea level is identified in the figure, and the location of the left and right rotors for an on-deck V-22 tilt-rotor. The island wake is well defined with an extensive area of reversed flow. An area of streamwise velocity defect above the island appears to originate from the funnels above the island. Local acceleration of the free-stream velocity is in evidence alongside the ship. The level of acceleration is comparable to the nominal blockage ratio of 6% mentioned earlier.

Figure 10 shows the lateral motion of the ship stern across the fixed field of view of the cameras as the ship is yawed, consistent with Figure 6. At 5 deg yaw, shown in Figure 10(b), significant lateral velocities appear in the island wake, directed across the deck from starboard to port. The region of reversed flow in the island wake has grown significantly. Evidence of a deck vortex is clearly present on the windward side of the deck. As the ship yaw is increased to 10 deg the deck vortex becomes more organized and the in-plane velocity vectors of Figure 10(c) clearly indicate this. A leeward vortex is now clearly present off the starboard side of the deck. As the ship yaw is increased to 15 deg, the flow complexity increases substantially. A strong clockwise (CW) windward vortex is shown lying above the deck in Figure 10(d) and a strong CW leeward vortex is visible off the starboard side. Downstream of the island a strong counter-clockwise (CCW) vortex has been established, no doubt being driven by the CW vortices on either side. This vortex would be important for Landing Spot 9 located downstream of the island on the starboard side of the deck.

The flow in Figure 10, above and to the right of the island, appears to be a little chaotic. This is attributed to the population of 100 frames being, perhaps, too low. Flow quality in the wake of the island and to the left of the island appears to be quite acceptable however. Fortunately, the current study is focused on the deck area at Landing Spot 7 located on the port side of the deck. Note that the apparent cross-sectional deck width grows with increase in ship yaw as the (fixed) LLS cuts the deck at an oblique angle.

Figure 10 documents a streamwise velocity ranging from reversed-flow velocities encountered in the island wake to levels greater than free stream along the port side of the deck. To enhance the more subtle velocity gradients in the current area of interest directly above the ship deck, Figure 11 presents the same data with a slightly different color palette, where streamwise velocities above 50% of free stream have been emphasized.

Measurement of the ship-alone air wake provides information on the inflow into the rotor disks of an on-deck tilt-rotor for any landing spot of choice. This information can be used to validate ship air-wake calculations and as input data to analyses for predicting the contribution to on-deck tilt-rotor forces and moments due to the ship-alone air-wake. These measurements also act as the baseline from which to measure the influence of an upwind aircraft on the on-deck tilt-rotor.

Ship + tandem-rotor helicopter wake, 0 deg yaw

In order to simulate a clean deck for the PIV measurements of the combined ship plus tandem-rotor helicopter wake at Spot 7, the on-deck tilt-rotor at Spot 8 remained unpowered. Any upstream influence of the stationary on-deck tilt-rotor at Spot 8 (Figure 4) on the PIV measurement plane at Spot 7 is assumed negligible.

Figure 12 illustrates the effect of changing the streamwise position of the UW aircraft ahead of the LLS at Landing Spot 7. Mean in-plane velocity components (normalized with the wind speed) are presented in the form of vectors and mean out-of-plane

velocity component in the form of a color-coded contour plot. Only 25% of the in-plane velocity vectors are shown for clarity. Figure 12 shows flowfield measurements at Spot 7 for 0 deg yaw and wind speed of 19.7 ft/sec (equivalent full-scale velocity of 35 knots). The island profile and the deck outline are included for clarity. The fore and aft rotor disks of the UW tandem-rotor helicopter are shown in blue. The downwash imposed on an on-deck tilt-rotor at Spot 7 can be determined by identifying the position of the left and right V-22 rotors in black.

Figure 12(a) shows the flowfield at Spot 7 for the UW tandem-rotor helicopter adjacent to Spot 6 with a lateral offset of 2(b/2) and a full-scale WHOD of 10 ft. The UW aircraft and its support hardware block the island wake from view. For this UW aircraft elevation, the aft rotor tip-path-plane is 7.52 in above the ship deck (equivalent full-scale height of 30.1 ft). The UW aircraft C_T is 0.0048. The condition described by Figure 12(a) is a useful reference point from which to study the effect of moving the UW aircraft in 3D-space on the velocity field at Spot 7.

In Figure 12(a) the wake from the UW helicopter is shown off the port side of the deck, located symmetrically behind the tandem-rotor helicopter. Note the single counter-rotating vortex pair. Each rotor disk of the tandem-rotor helicopter is assumed to generate a wake that resembles, in many respects, the wake from a fixed wing. Unlike the tightly rolled up tip vortices that form downstream from a fixed-wing aircraft, each rotor disk is assumed to generate a pair of "super vortices". These vortices are much larger in physical size and are assumed to take longer for complete roll-up to occur than for a fixed wing aircraft. Due to the proximity of the two rotor disks, the tandem-rotor helicopter generates only a single pair of super vortices. The trailed vortices from the forward rotor disk amalgamate with and reinforce those from the aft rotor disk. Note the large in-plane velocities associated with the rotor wake. The starboard super vortex from the UW helicopter is apparently weaker than the port super vortex. The starboard super vortex is located above the port edge of the deck and viscous forces (the deck boundary layer) will dissipate the rotational energy of this vortex. Although both super vortices are associated with an increase in streamwise velocity component (more than 50% for the port vortex) the starboard super vortex exhibits a local velocity defect in the core. The streamwise velocity defect observed in a narrow vertical band between the two super vortices from the UW helicopter identifies the wake from the streamlined vertical strut supporting the UW aircraft.

The effect on the flowfield at Spot 7 of moving the UW aircraft to the next upwind landing area at Spot 5 is shown in Figure 12(b), keeping all other conditions constant (namely UW aircraft C_T, lateral offset of UW aircraft, WHOD, yaw angle and wind speed). Fortunately the UW model and its support hardware no longer block the camera view. The island wake is revealed in great detail and displays an extensive region of reversed flow. Since the landing area at Spot 7 is of primary concern (rather than the island wake) streamwise velocity components below 50% of free-stream are not presented in order to improve the contour plot sensitivity in the vicinity of free-stream. As the UW aircraft moves forward ahead of the LLS location, the effective "age" of the rotor wake being measured increases and the rotor wake can be expected to descend. Figure 12(b) confirms the expected descent of the rotor wake with increasing distance between the generating aircraft and the measurement plane. The excess streamwise velocity associated with each super vortex has evidently diminished. A streamwise velocity defect is now associated with the starboard vortex. Figure 12(c) confirms that as the UW aircraft moves upwind to yet another landing area at Spot 4, the descent of the UW aircraft wake with increasing downstream distance from the generating aircraft continues. Figure 12(c) indicates that both super vortices now lie below the level of the ship deck and are therefore in the shadow of the LLS (no data available). Figures 12(a) through 12(c) also reveal that the helicopter wake moves progressively outboard, away from the ship, with increasing wake age.

Figure 13 illustrates the effect on the flowfield at Landing Spot 7 as the lateral offset of the UW helicopter from Landing Spot 6 is varied. Full-scale WHOD is 10 ft and the UW helicopter C_T is 0.0048. Figure 13(b) represents the flowfield associated with the reference condition with lateral offset 2(b/2) previously presented in Figure 12(a) and described immediately above.

In Figure 13(c) the UW helicopter is at an increased lateral offset of 4(b/2) from Spot 6. In-plane velocity vectors clearly indicate strong entrainment into the island wake from either side of the island and from above the island. This is dictated by wake closure downstream of the island. The wake from the UW helicopter is shown off the port side of the deck. Note the single counter-rotating vortex pair and the large in-plane velocities (comparable to the free stream velocity) associated with the rotor wake. Note also the local acceleration of the wind in the free stream direction to more than 50% above free stream. Evidence of the strut wake can be seen in the streamwise velocity defect between the two super vortices. Despite the fact that most of the flowfield of interest (above the deck) is obscured from view by the UW model and support hardware, downwash from the rotor wake clearly has little effect above the deck of the ship. In moving the UW aircraft further from the deck, the tandem-rotor

helicopter wake has become more closely symmetric because the starboard super vortex is less affected by the deck boundary layer.

Figure 13(a) describes perhaps the most interesting situation where the UW helicopter has moved directly above Spot 6 (lateral offset = 0) placing the UW aircraft at the landing spot immediately upwind from the measurement station. The wake from the vertical streamlined strut supporting the UW aircraft is now clearly visible as a region of reduced streamwise velocity extending vertically from between the two super vortices. This can be used to identify the approximate location of the plane of symmetry of the UW aircraft. The starboard super vortex is seen to have moved laterally across the deck --- probably a combination of entrainment into the island wake and mutual induction between this vortex and its mirror image in the ship deck (ship deck acts like a plane of symmetry). The starboard super vortex exhibits no streamwise velocity excess whatsoever. The island wake is severely deformed by interaction with this super vortex. The port super vortex has diminished streamwise velocity excess possibly from entrainment of the ship boundary layer.

Figure 14 explores the effect of changing the vertical height of the upwind aircraft. Figure 14(a) is the same as Figures 12(a) and 13(b). Figure 14(a) has the upwind aircraft adjacent to Spot 6 with lateral offset 2(b/2) and WHOD = 10 ft. The island wake is blocked from view by the UW model and its associated hardware. Presence of the starboard super vortex above the edge of the deck appears to pull low momentum fluid from behind the island and result in an enhanced streamwise boundary layer thickness above the deck. The starboard super vortex is seen to pass beneath the left rotor of an on-deck tilt-rotor. Figure 14(b) represents a WHOD of 25 ft. The UW model no longer obscures the lower part of the island wake. As the UW model is raised, the trailed wake follows. The starboard super vortex has increased in strength as it moved off the deck, and the velocity defect at the core is no longer present. The starboard super vortex now lies in the plane of the left rotor of an on-deck tilt-rotor. Notably, this corresponds to a peak in the observed on-deck tilt-rotor rolling moment, left wing down (see Ref. 2). Increasing the wheel height over deck still further to WHOD = 40 ft, Figure 14(c) reveals more of the island wake and results in a more nearly symmetric rotor wake. The starboard super vortex now passes above the left rotor of an on-deck tilt-rotor at Spot 7.

Ship + tandem-rotor helicopter wake, 15 deg yaw

It is instructive to re-visit Figure 11, which illustrates the main difference between zero and 15 deg yaw is in the strength of the deck vortex at 15 deg yaw. This has a significant effect on the combined flowfield. The island wake is extremely complex, especially the interaction between the island wake and the lee-side deck vortex. The present paper, however, is primarily interested in the flowfield above Spot 7 with direct application to the roll-on-deck phenomenon at that spot. Detailed presentation of the island wake has therefore been sacrificed in order to concentrate on the area above the deck adjacent to the island wake since this defines the flowfield for Landing Spot 7. The non-dimensional out-of-plane velocities are therefore restricted to the range 0.50 to 1.50 in the color-coded contour plots.

The UW aircraft position is first moved streamwise, then laterally, and finally vertically for a ship (and UW aircraft) yaw angle of 15 deg (to starboard) and wind speed of 19.7 ft/sec (equivalent full-scale wind speed of 35 knots). Figure 15 illustrates the effect on the velocity field at Spot 7 as the UW aircraft is moved in the streamwise direction. The data shown in Figure 15 correspond to an UW aircraft displacement somewhat more complex than a simple translation of the UW aircraft in the streamwise direction. Due to the ship yaw (to starboard) as the UW aircraft moves forward the rotor wake impinges on the ship at an earlier station. To maintain the UW rotor wake at about the same position above the ship deck in the plane of the PIV measurement station at Spot 7, a compound move of the UW aircraft is performed (see figure legend for details). Figure 15(a) illustrates the velocity field at Spot 7 with the UW aircraft adjacent to Spot 6 (the closest UW landing spot to the PIV plane) with a lateral offset of 2(b/2) measured perpendicular to the axis of the ship. This test condition defines the reference position for a series of PIV measurements at 15 deg yaw. Motion of the UW aircraft relative to this position is used to try and understand the flowfield development better.

In Figure 15(a) the wake of the UW tandem-rotor helicopter is revealed as a pair of counter-rotating super vortices. The port vortex is seen to rotate in the CW sense and the starboard vortex in the CCW sense when viewed looking upstream. Both super vortices are seen to be associated with a region of excess streamwise velocity surrounding the core which exhibits a streamwise velocity defect (more clearly visible in the starboard vortex). A strong deck vortex is clearly visible rotating in the CW sense. Note that the starboard super vortex passes above the rotor plane of an on-deck tilt-rotor. The proximity of the starboard super vortex to the rotor plane of the on-deck tilt-rotor indicates strong downwash on the left rotor and strong upwash on the right rotor. Similarly, the port super vortex produces a strong downwash on the left rotor. The deck vortex also produces upwash at the right rotor. Reduced thrust is therefore expected from the left rotor and increased thrust from the right rotor. A strong rolling moment, left

wing down, is indicated. This was borne out by on-deck force and moment measurements (see Ref. 2).

Figure 15(b) illustrates the effect of the UW aircraft moving upwind to the next landing spot (Spot 5) with a lateral offset of 3(b/2). Note that the port vortex from the UW aircraft has descended slightly whilst the starboard vortex has risen significantly. The rotor wake has a natural tendency to descend as it moves rearwards, explaining the behavior of the port vortex. The starboard super vortex and the deck vortex are quite close together and mutual induction results in their ascent above the ship deck. The streamwise velocity defect on the axis of the starboard super vortex is seen to increase compared to Figure 15(a) and the area occupied by the region of velocity defect in the vicinity of the core has grown significantly. Figure 15(c) represents the velocity field at Spot 7 due to the UW aircraft moving further upwind to Spot 4 with a lateral offset of 4(b/2). The port super vortex from the UW aircraft continues its descent and the starboard super vortex and the ship deck vortex continue their ascent above the ship deck. The lee vortex that becomes established off the starboard side of the deck appears to entrain flow from the island wake. The island wake is a region of high streamwise velocity defect. This low momentum fluid appears to migrate towards the center of this lee vortex.

Figure 16 illustrates the effect of changing the lateral position of the UW aircraft. Figure 15(a) is presented again as Figure 16(b). Figure 16(c) illustrates the effect of moving the UW aircraft further outboard from the ship at Spot 6. The port super vortex is now out of the field of view on the LHS of the image. Immediately adjacent to the left-hand boundary of the flowfield can be seen the wake of the support strut. The starboard super vortex has increased excess streamwise velocity associated with it compared to Figure 16(b). The increased lateral separation between the CCW starboard super vortex and the CW deck vortex results in limited mutual induction, with the result that the ship deck vortex remains attached to the deck. Figure 16(a) illustrates the effect of moving the UW aircraft inboard so that it is immediately above the landing spot at Spot 6. An extensive area of streamwise velocity defect is seen to be associated with the center of the starboard super vortex. No evidence of the CW deck vortex can be seen. It is assumed that the CCW starboard super vortex has merged with the CW deck vortex. The result appears to be a much smaller (and weaker) CCW vortex that lies close to the ship deck.

Figure 17 illustrates the effect of changing the height of the UW tandem-rotor helicopter. Figure 17(a) is identical to Figures 15(a) and 16(b). This flowfield has already been described in discussing Figure 15(a). Figure 17(b) shows the effect of increasing the UW aircraft full-scale elevation to WHOD = 25 ft. A clearer picture of the isolated UW aircraft wake is starting to appear. Each super vortex is associated with a region of excess streamwise velocity (above free stream) and the counter-rotating super vortices are connected by a similar band of high streamwise velocity beneath the vortex pair. The velocity defect in the core of the starboard vortex has almost disappeared. The starboard super-vortex is higher than the port super-vortex due to mutual induction between the starboard vortex and the ship deck vortex. In Figure 17(c) the full-scale WHOD has been raised to 40 ft. At this elevation above the ship deck, the UW aircraft wake passes well above the rotor plane of an on-deck tilt-rotor. Associated downwash through the rotor plane of an on-deck tilt-rotor is clearly reduced with increasing WHOD of the UW aircraft.

Concluding Remarks

The aerodynamic interaction between a tandem-rotor helicopter and an amphibious assault ship has been quantified using three-component PIV velocity field measurements. Using 1/48th-scale models in the U.S. Army 7- by 10-Ft Wind Tunnel at NASA Ames, the wake of the isolated ship and the combined wake of the ship and helicopter have been separately documented. Test conditions included variations in wind speed, ship yaw angle, and position of the helicopter. Since the primary motivation for this experiment was to understand the aerodynamic interactions influencing an on-deck V-22 with aircraft operating upwind, the PIV data were acquired in a cross-flow plane coincident with a vertical plane passing through the rotor centers of an on-deck tilt-rotor (without the presence of the tilt-rotor).

For isolated-ship conditions, the PIV data clearly show the effects of ship yaw angle on deck vortex strength and location. The PIV data from the combined ship and helicopter configurations identify the location of the convected helicopter wake as the rotor wake passes over a landing spot typically used by tilt-rotors. The rotor wake position highlights the physics underlying a potential uncommanded roll experienced by an on-deck tilt-rotor. The 1/48th-scale ship and rotorcraft models together with the PIV technique have provided a wealth of information on the aerodynamic interaction of a helicopter operating in proximity to a ship. Data from this experiment provide a benchmark for CFD analysis validation. Information provided by this experiment will be extremely useful in guiding the safe operation of various rotorcraft configurations aboard a ship.

Acknowledgements

The authors gratefully acknowledge support from the test crew at the U.S. Army 7- by 10-Foot Wind Tunnel at NASA Ames Research Center. The U.S. Navy V-22 Program Office provided funding for this helicopter-ship interaction study.

References

1. Wall, Robert, "MV-22, Back at Sea, Tackles More Tests," *Aerospace Daily*, January 20, 2003.

2. Silva, M. J., Yamauchi, G. K., Wadcock, A. J. and Long, K. R., "Wind Tunnel Investigation of the Aerodynamic Interactions Between Helicopters and Tiltrotors in a Shipboard Environment," American Helicopter Society Aeromechanics Specialist's Conference, San Francisco, CA, January 2004.

3. Yamauchi, G. K., Wadcock, A. J., Derby, M. D. and Long, K. R., "Results from the V-22/Ship/Helicopter Aerodynamic Interaction Phenomena (VSHAIP) Wind Tunnel Test," NASA TM to be published, 2004.

4. Abrego, A. I. and Long, K. L., "A Wind Tunnel Investigation of a Small-Scale Tiltrotor Model in Descending Flight," American Helicopter Society Aerodynamics, Acoustics, and Test and Evaluation Technical Specialists Meeting, San Francisco, CA, January 2002.

5. Abrego, A. I., Betzina, M. D., and Long, K. L., "A Small-Scale Tiltrotor Model Operating in Descending Flight," 28th European Rotorcraft Forum, Bristol, United Kingdom, September 2002.

6. Derby, M. R. and Yamauchi, G. K., "Design of 1/48th-Scale Models for Ship-Rotorcraft Interaction Studies," AIAA-2003-3952, 21st AIAA Applied Aerodynamics Conference, Orlando, FL, June 2003.

7. Johnson, W., Yamauchi, G. K., Derby, M. D., and Wadcock, A. J., "Wind Tunnel Measurements and Calculations of Aerodynamic Interactions Between Tiltrotor Aircraft," AIAA-2003-47, 41st AIAA Aerospace Sciences Meeting and Exhibit, Reno, NV, January 2003.

8. Yamauchi, G. K., Wadcock, A. J. and Derby, M. R., "Measured Aerodynamic Interaction of Two Tiltrotors," American Helicopter Society 59th Annual Forum, Phoenix, AZ, May 2003.

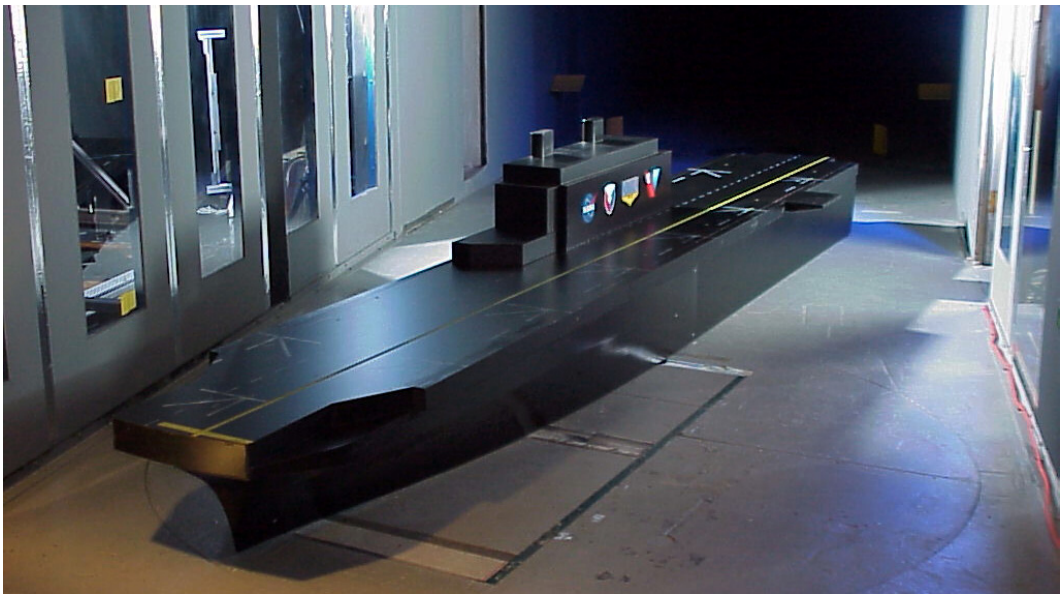

Figure 1. 1/48th-scale amphibious assault ship installed in 7- by 10-Foot Wind Tunnel at NASA Ames.

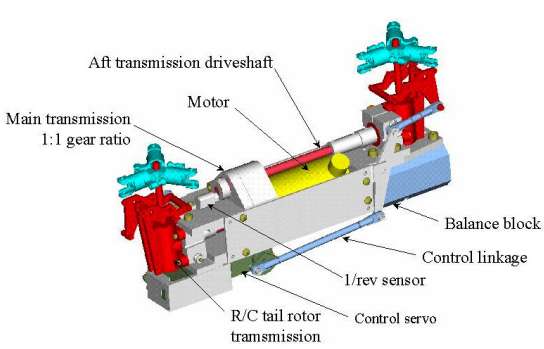

(a) Major components of tandem-rotor helicopter.

(b) Tandem-rotor helicopter mounted on sting.

Figure 2. Tandem-rotor helicopter model.

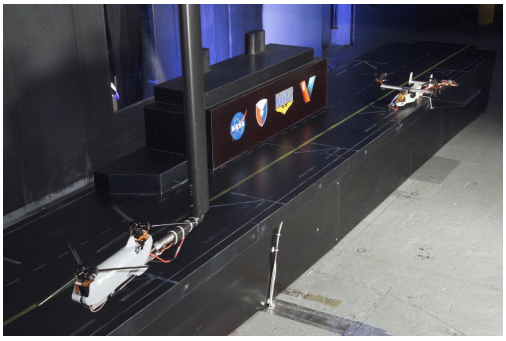

Figure 3. Model installation in Army 7- by 10-Foot Wind Tunnel. On-deck tilt-rotor at Spot 7.

Figure 4. On-deck model tilt-rotor at Spot 8.

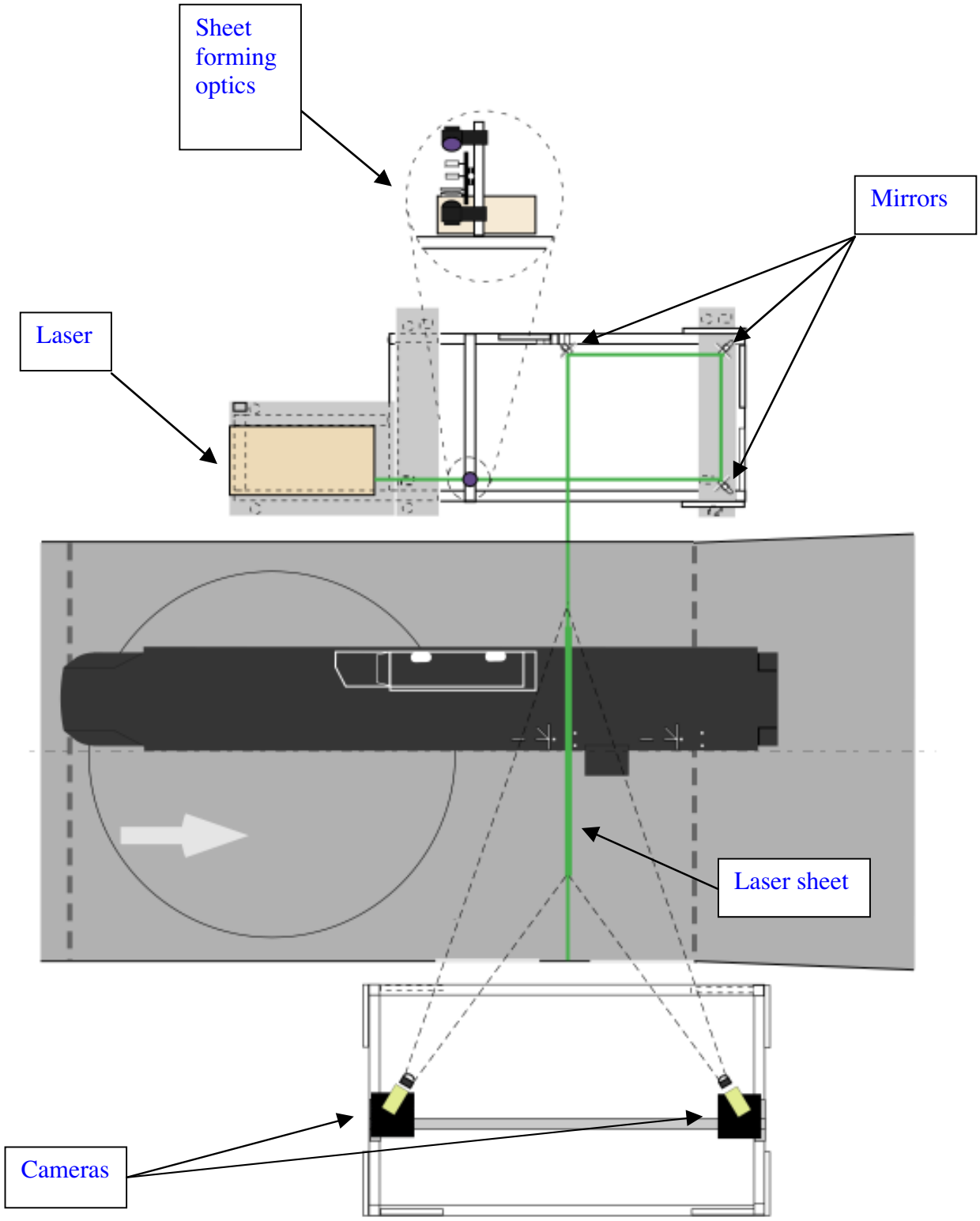

Figure 5. Plan view of PIV set-up in the 7- by 10-Ft Wind Tunnel.

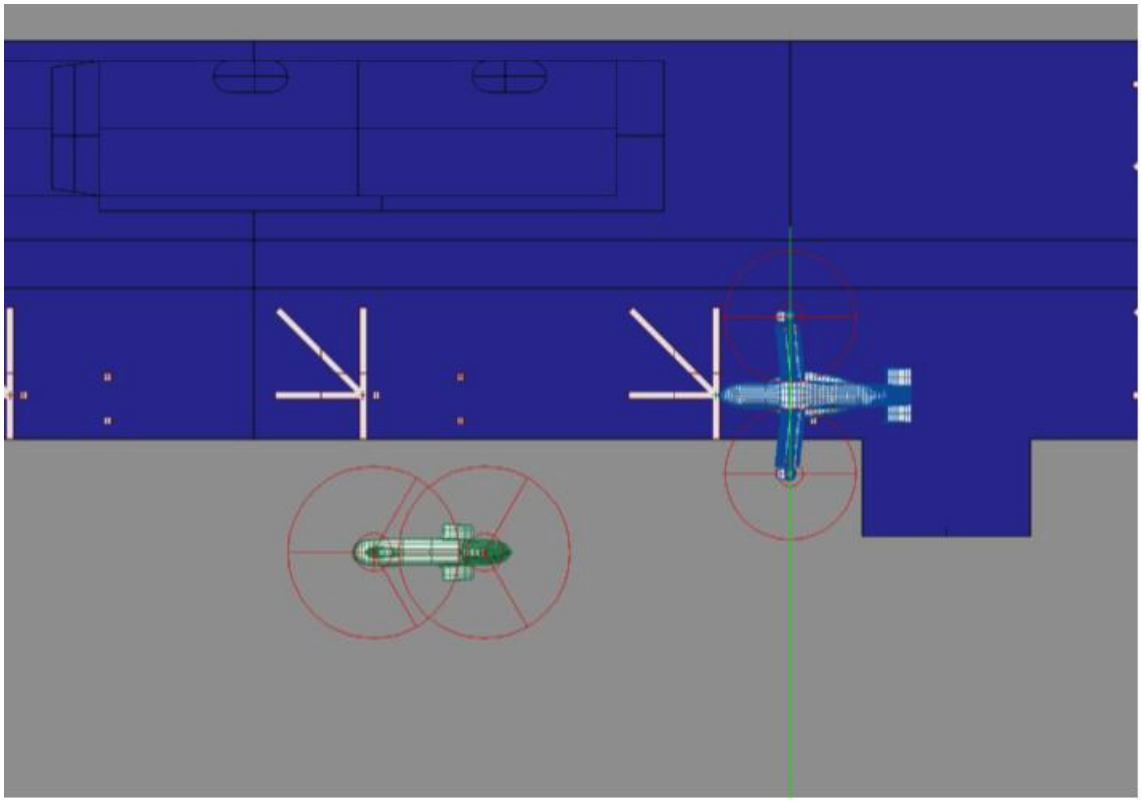

(a) On deck V-22 at Spot 7. Ship and UW model yaw = 0 deg.

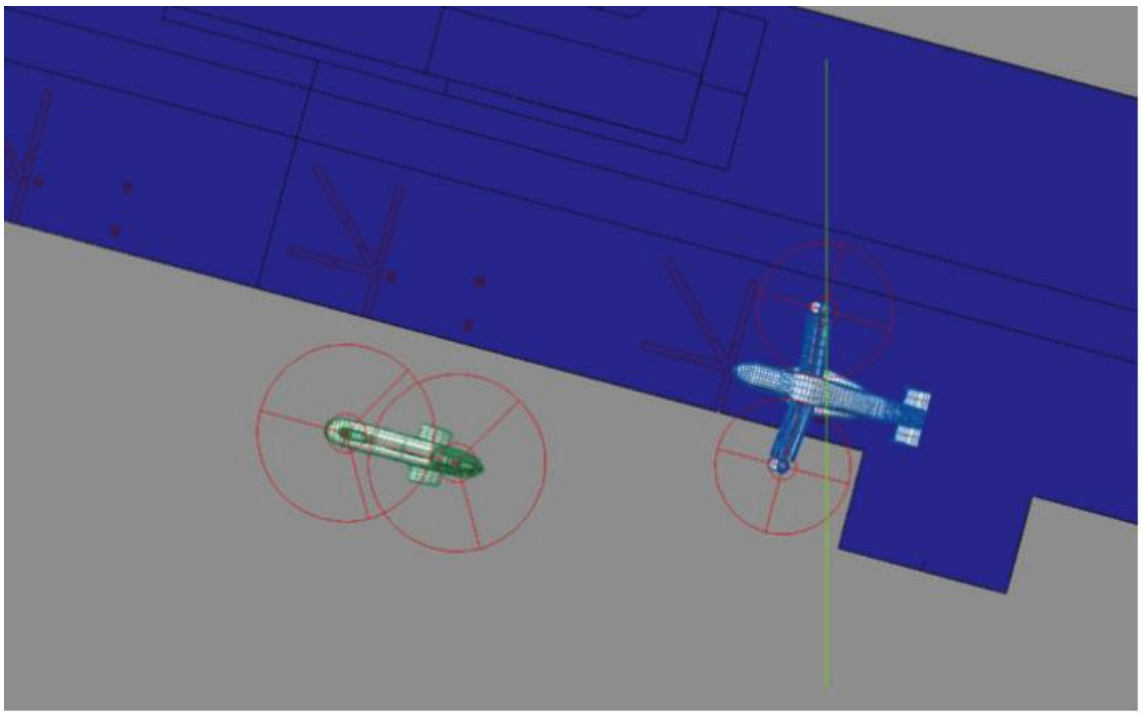

(b) On deck V-22 at Spot 7. Ship and UW model yaw = 15 deg.

Figure 6. LLS location in wind tunnel.

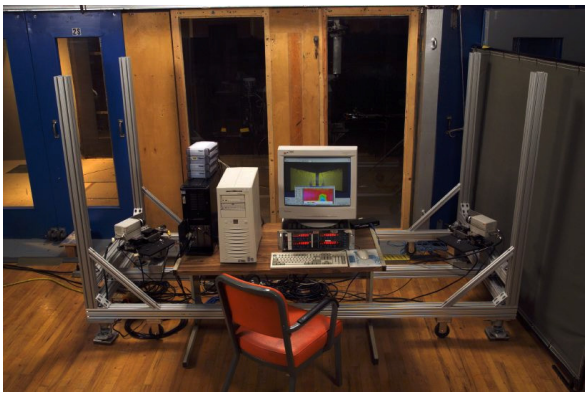

Figure 7. PIV cameras on rail-mounted frame outside test section.

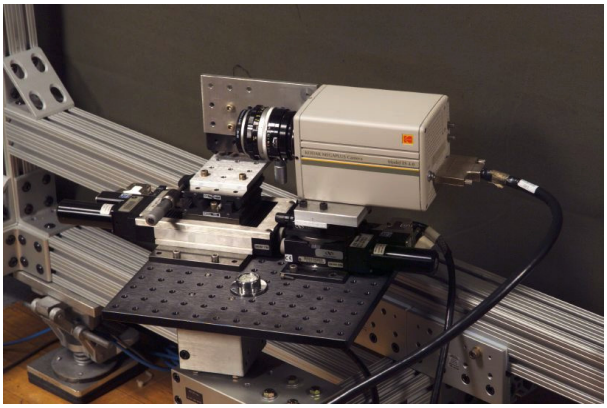

Figure 8. Close-up of PIV camera mount.

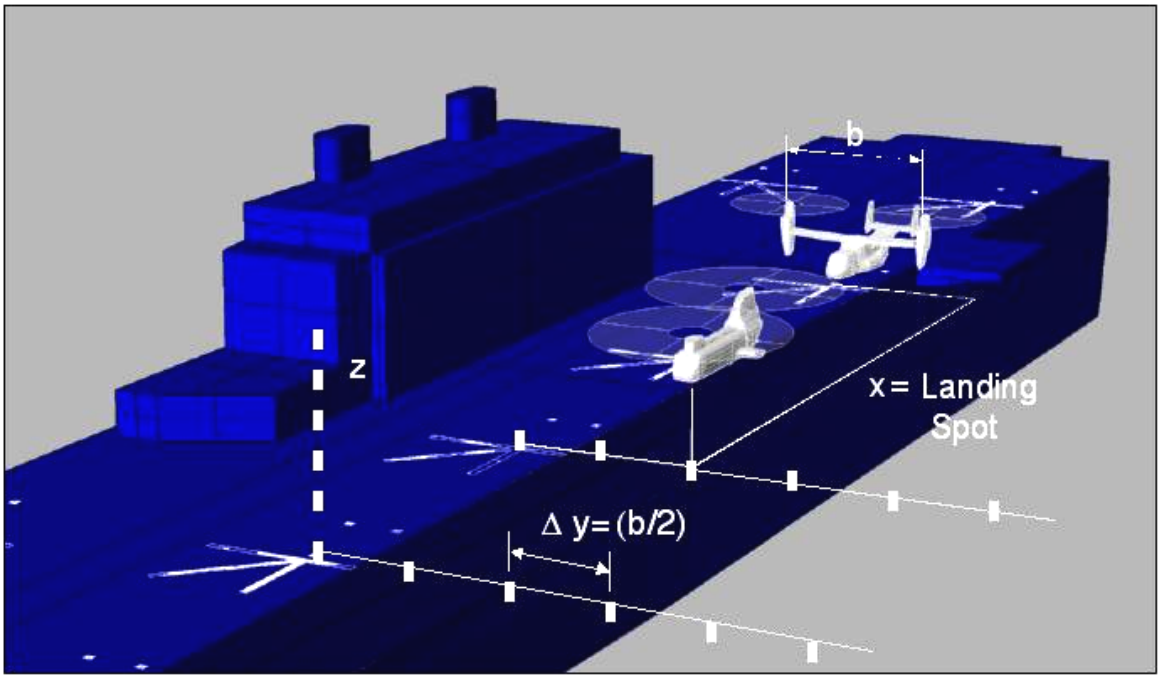

Figure 9. Geometry for mapping position of rotorcraft operating near or on the ship.

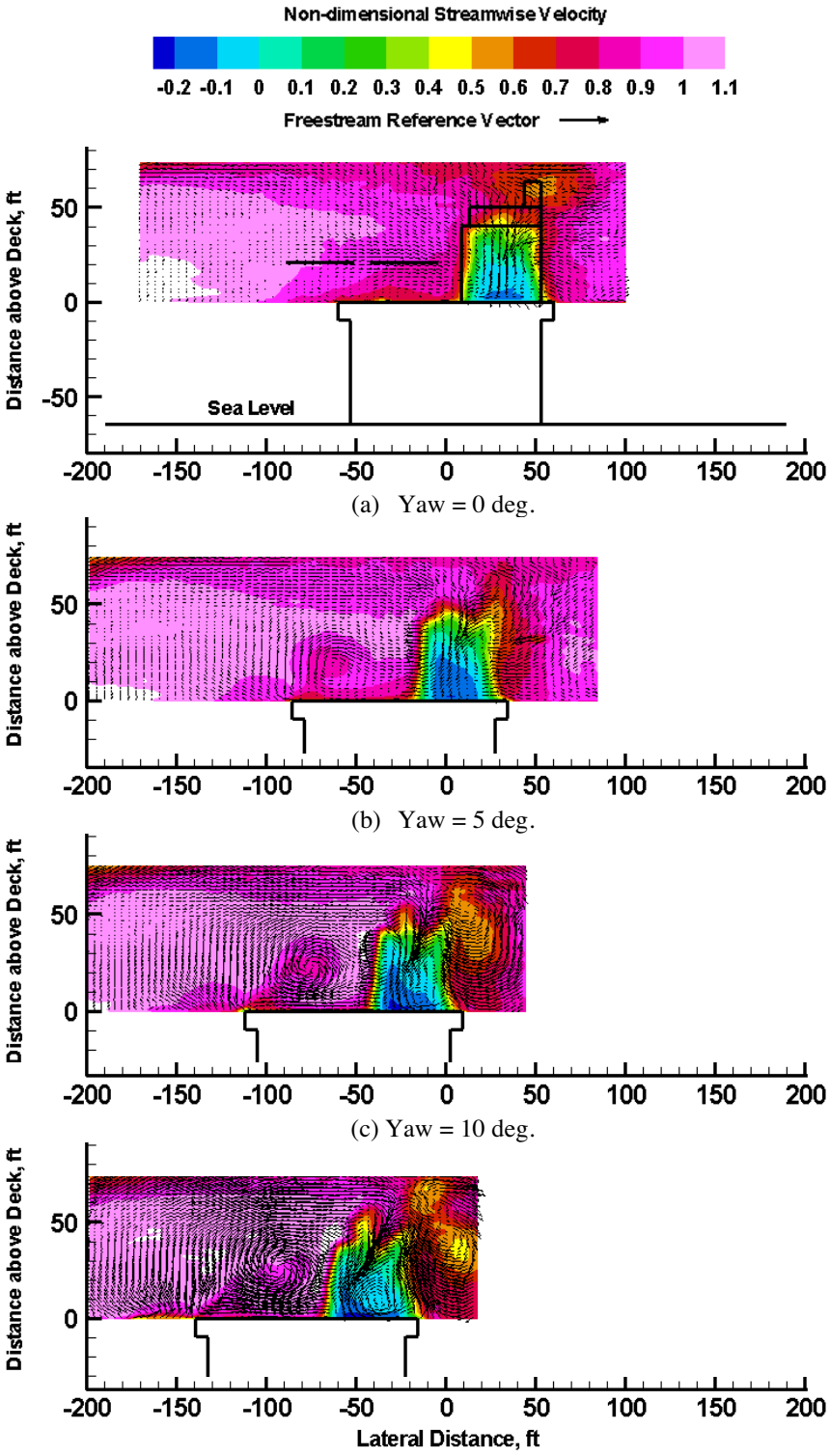

(a) Yaw = 0 deg.

(b) Yaw = 5 deg.

(c) Yaw = 10 deg.

(d) Yaw = 15 deg.

Figure 10. Ship-alone air-wake. Effect of ship yaw on velocity field at Spot 7. 25% of in-plane vectors plotted. Contour plot of out-of-plane velocity component. Wind speed = 22.5 ft/sec. View looking upstream.

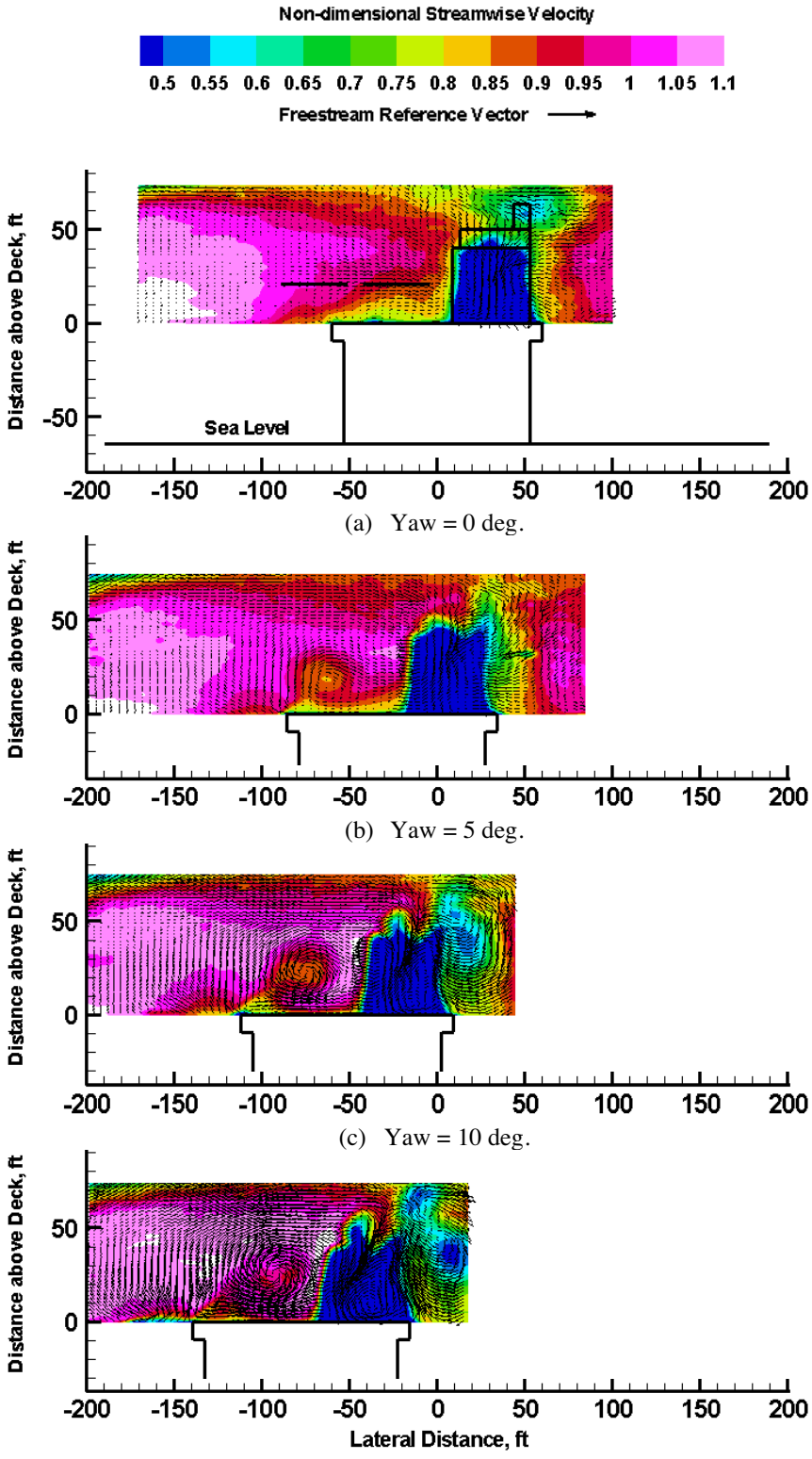

Figure 11. Ship-alone air-wake. Effect of ship yaw on velocity field at Spot 7. (Same data as Fig. 10, with different color key).

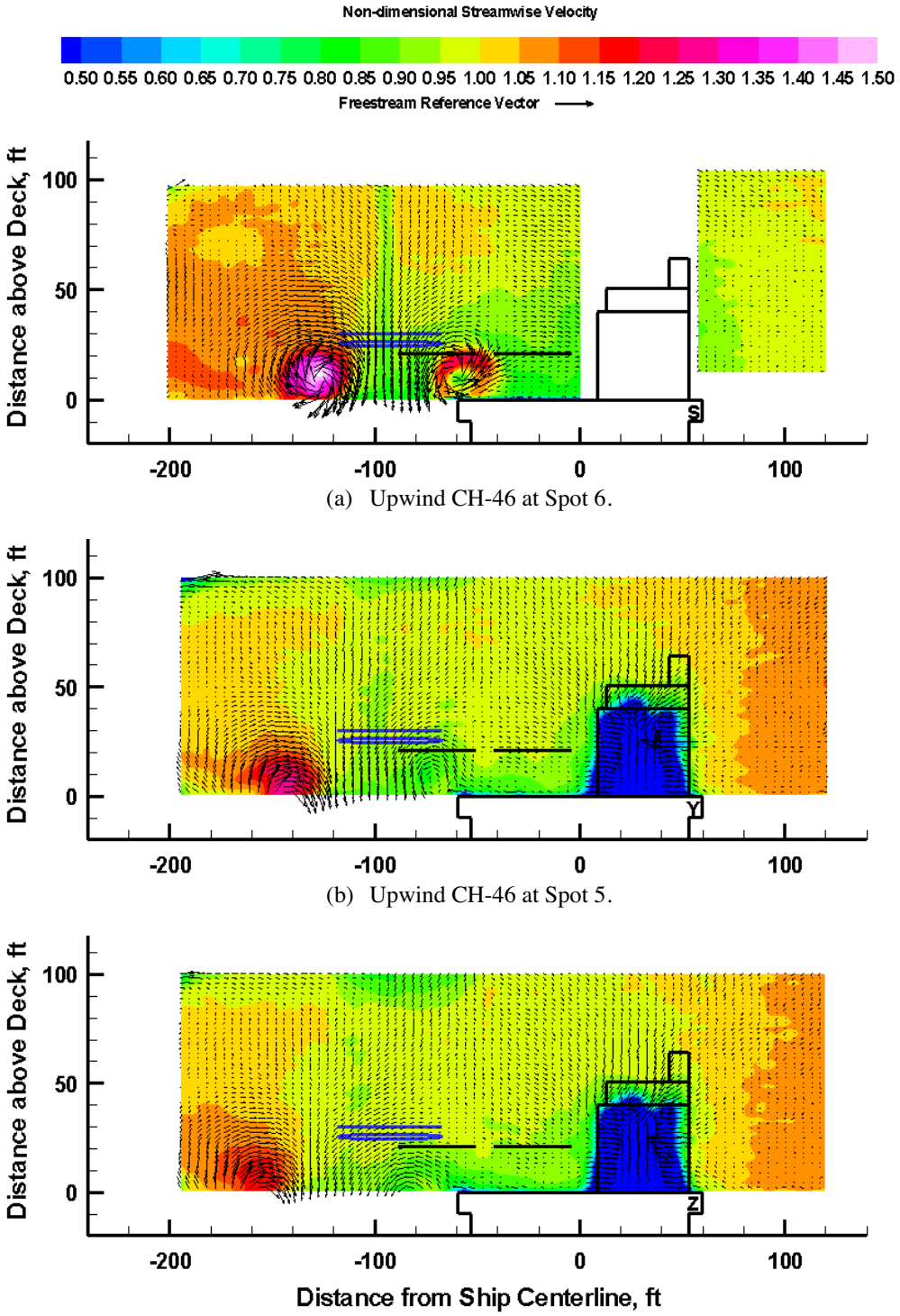

(a) Upwind CH-46 at Spot 6.

(b) Upwind CH-46 at Spot 5.

(c) Upwind CH-46 at Spot 4.

Figure 12. Combined wake. Effect of streamwise position of upwind CH-46 on velocity field at Spot 7.
25% of in-plane vectors plotted. Contour plot of out-of-plane velocity component.
Yaw = 0 deg, lateral offset = 2(b/2), WHOD = 10.6 ft.
Equivalent full-scale wind speed = 35 knots. View looking upstream.

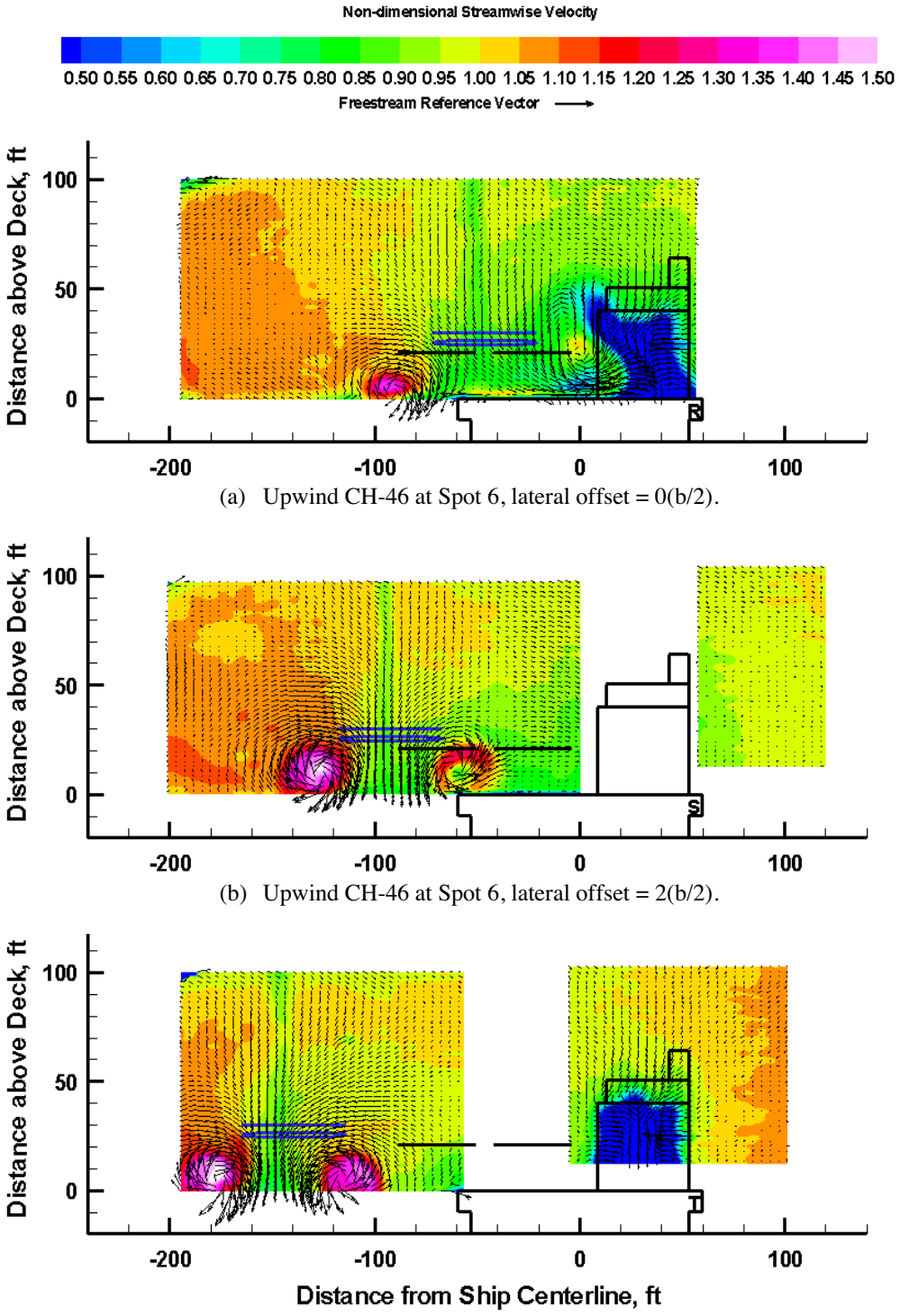

(a) Upwind CH-46 at Spot 6, lateral offset = 0(b/2).

(b) Upwind CH-46 at Spot 6, lateral offset = 2(b/2).

(c) Upwind CH-46 at Spot 6, lateral offset = 4(b/2).

Figure 13. Combined wake. Effect of lateral offset of upwind CH-46 on velocity field at Spot 7.
25% of in-plane vectors plotted. Contour plot of out-of-plane velocity component.
Yaw = 0 deg, CH-46 at Spot 6, WHOD = 10.6 ft.
Equivalent full-scale wind speed = 35 knots. View looking upstream.

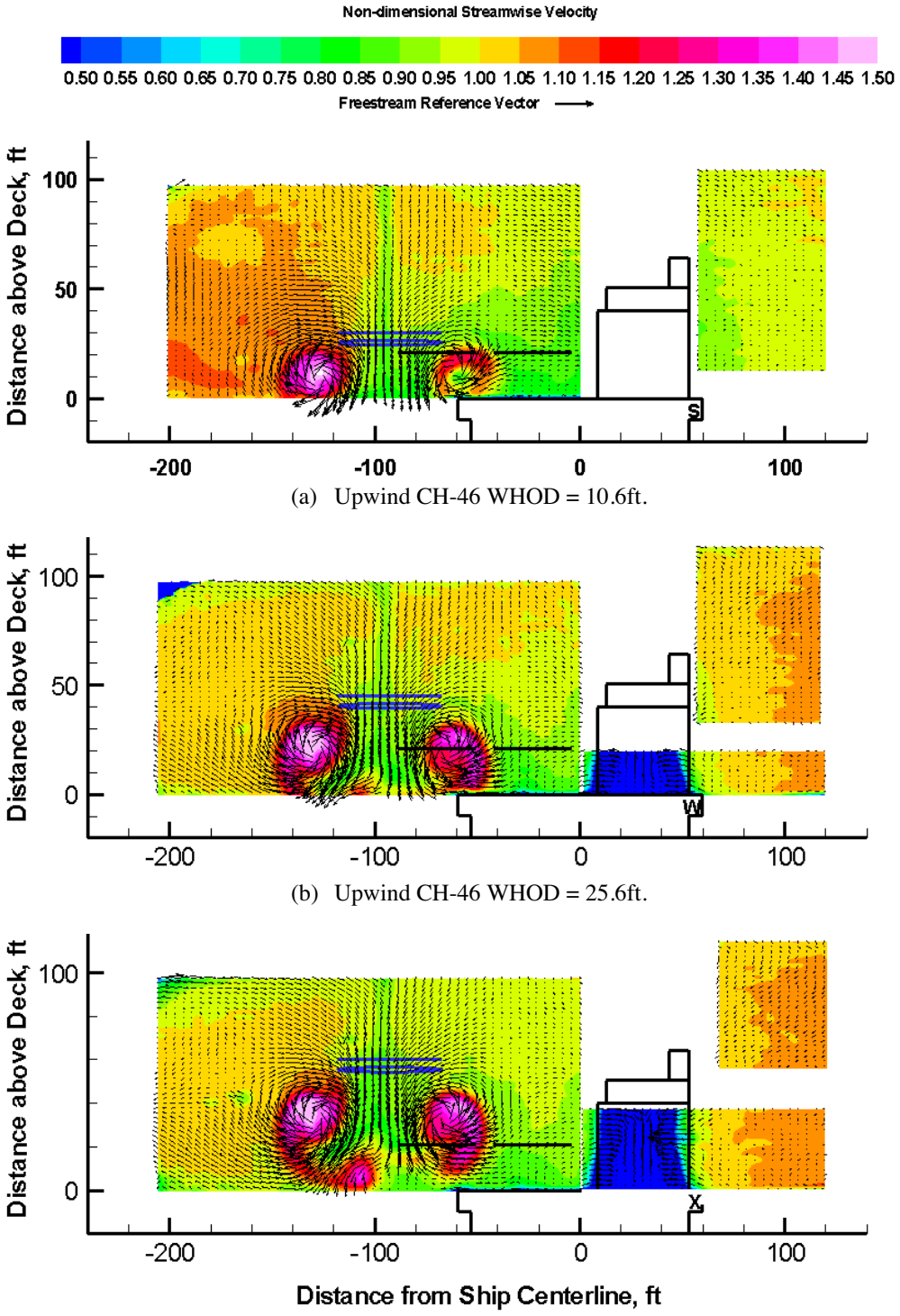

(a) Upwind CH-46 WHOD = 10.6ft.

(b) Upwind CH-46 WHOD = 25.6ft.

(c) Upwind CH-46 WHOD = 40.6ft.

Figure 14. Combined wake. Effect of vertical position of upwind CH-46 on velocity field at Spot 7. 25% of in-plane vectors plotted. Contour plot of out-of-plane velocity component. Yaw = 0 deg, CH-46 at Spot 6, lateral offset = 2(b/2). Equivalent full-scale wind speed = 35 knots. View looking upstream.

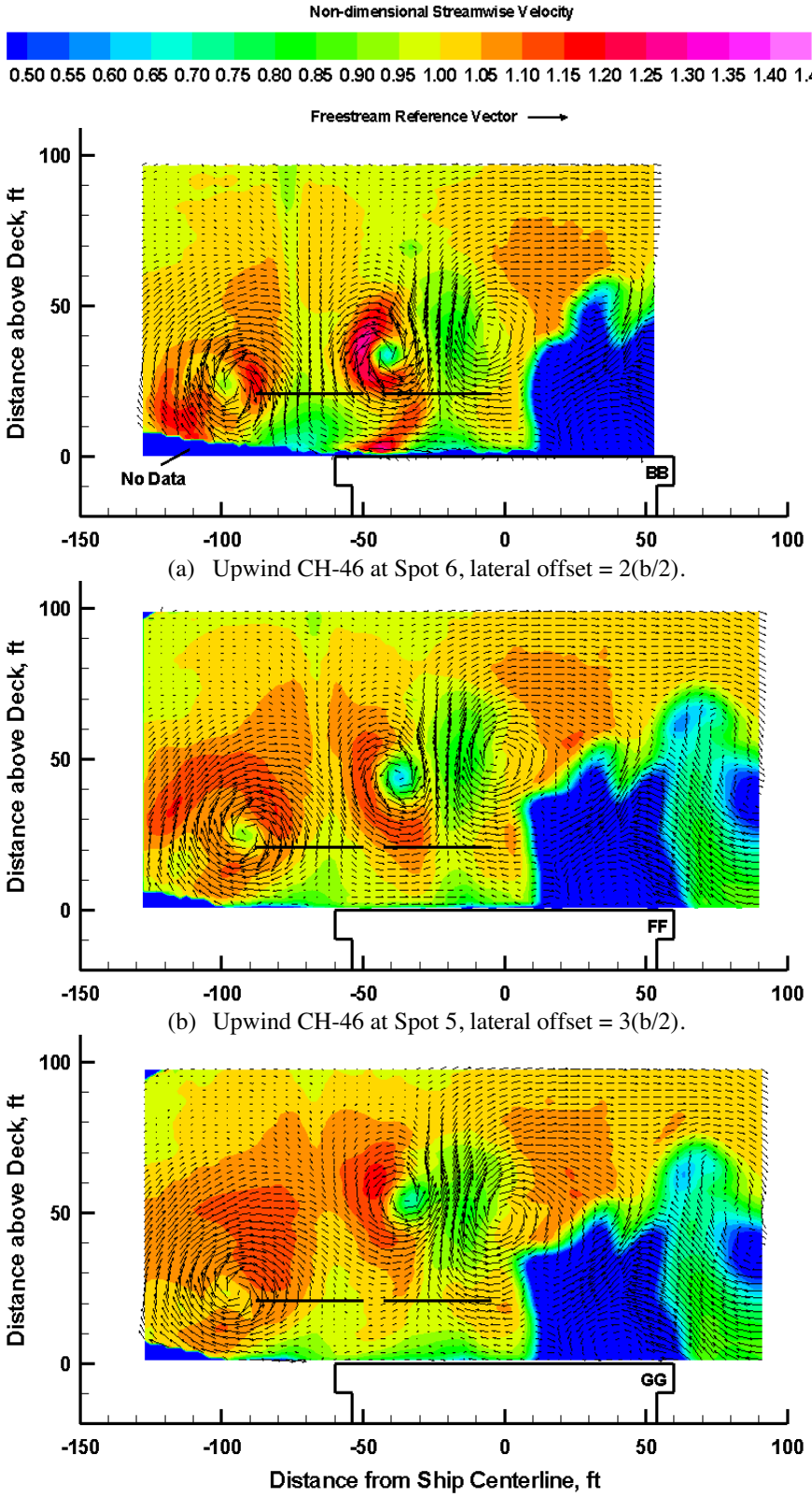

(a) Upwind CH-46 at Spot 6, lateral offset = 2(b/2).

(b) Upwind CH-46 at Spot 5, lateral offset = 3(b/2).

(c) Upwind CH-46 at Spot 4, lateral offset = 4(b/2).

Figure 15. Combined wake. Effect of streamwise position of upwind CH-46 on velocity field at Spot 7. 25% of in-plane vectors plotted. Contour plot of out-of-plane velocity component. Yaw = 15 deg (nose-right). CH-46 WHOD = 10.6 ft. Equivalent full-scale wind speed = 35 knots. View looking upstream.

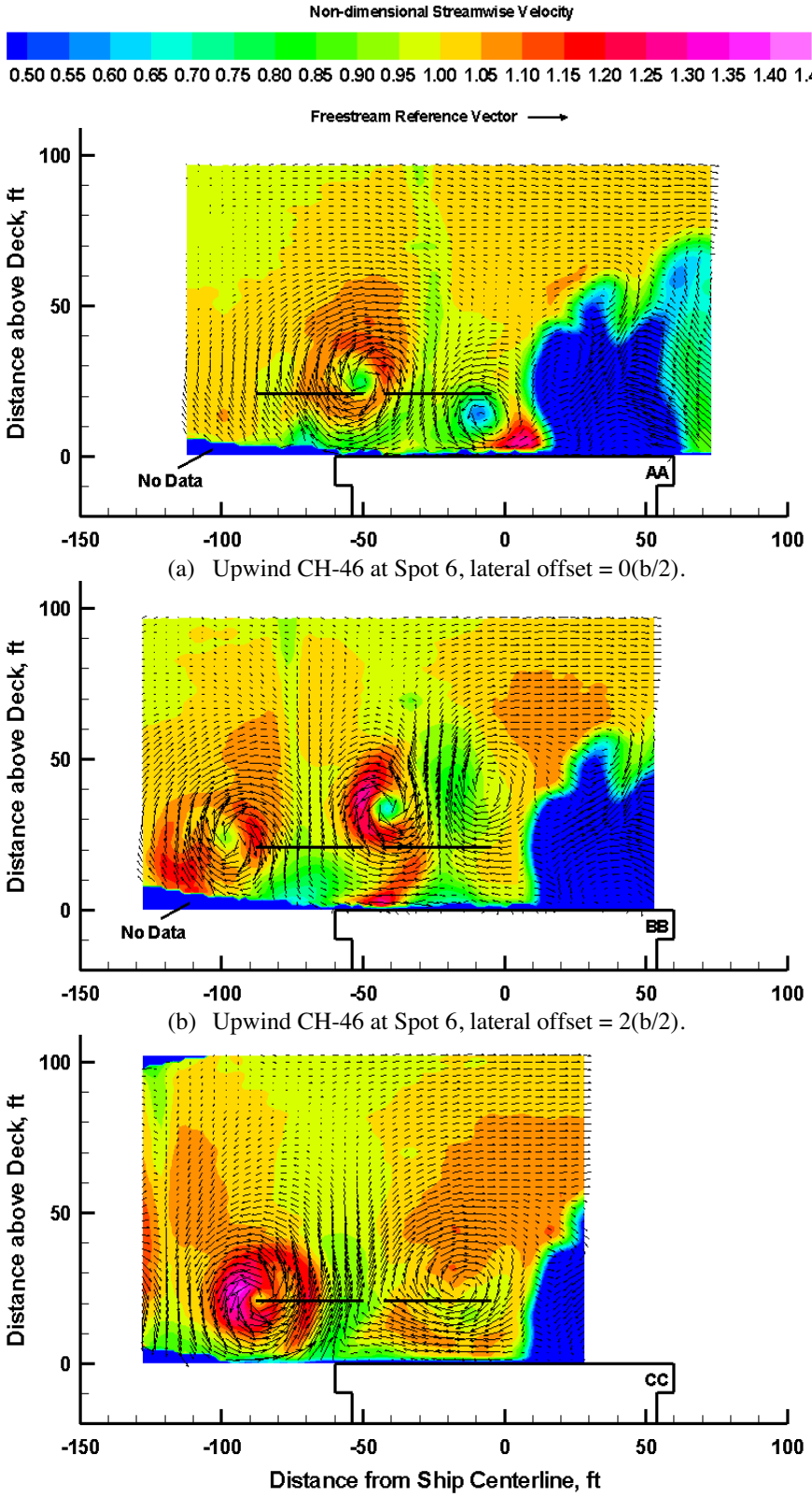

(a) Upwind CH-46 at Spot 6, lateral offset = 0(b/2).

(b) Upwind CH-46 at Spot 6, lateral offset = 2(b/2).

(c) Upwind CH-46 at Spot 6, lateral offset = 4(b/2).

Figure 16. Combined wake. Effect of lateral offset of upwind CH-46 on velocity field at Spot 7. 25% of in-plane vectors plotted. Contour plot of out-of-plane velocity component. Yaw = 15 deg (nose-right). CH-46 at Spot 6, WHOD = 10.6 ft. Equivalent full-scale wind speed = 35 knots. View looking upstream.

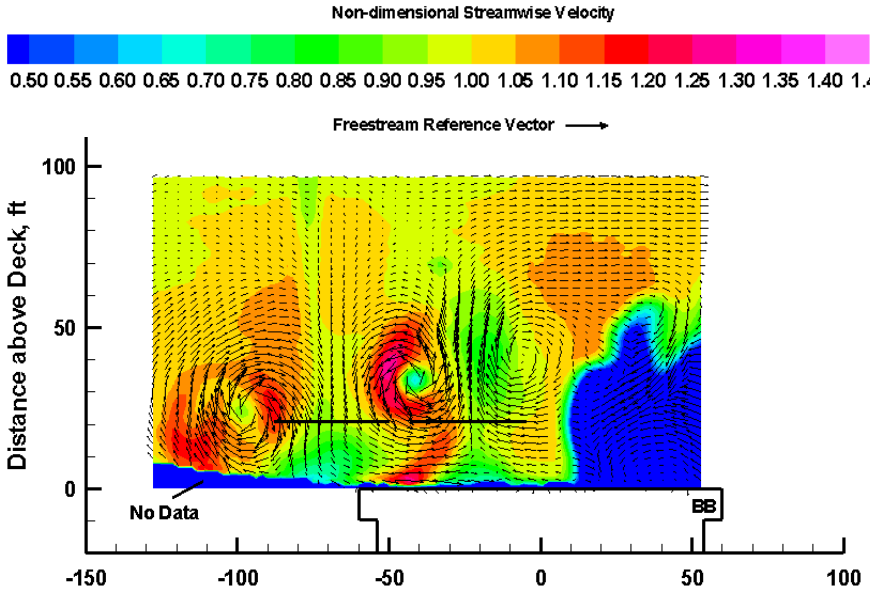

(a) Upwind CH-46 at WHOD = 10.6ft.

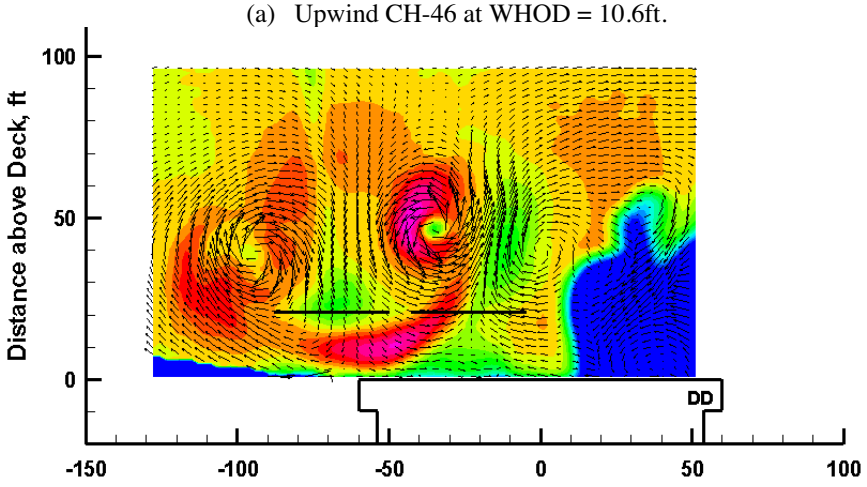

(b) Upwind CH-46 at WHOD = 25.6ft.

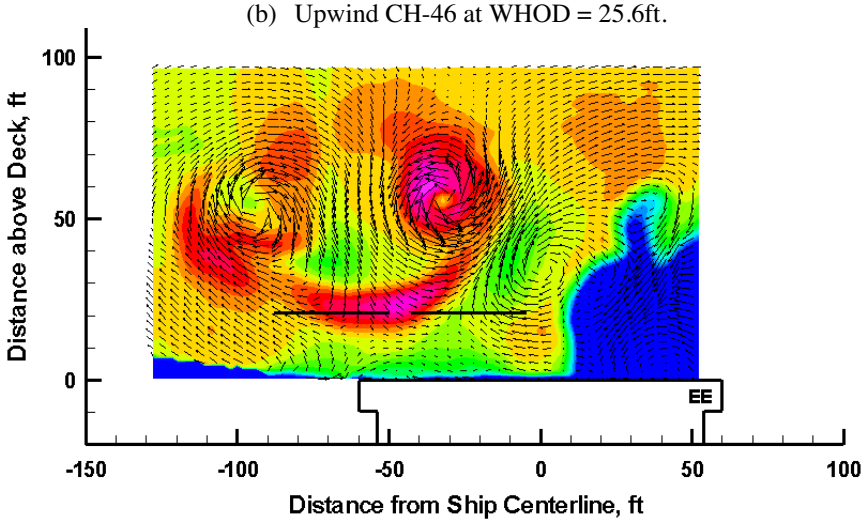

(c) Upwind CH-46 at WHOD = 50.6ft.

Figure 17. Combined wake. Effect of vertical position of upwind CH-46 on velocity field at Spot 7. 25% of in-plane vectors plotted. Contour plot of out-of-plane velocity component. Yaw = 15 deg (nose-right). CH-46 at Spot 6, lateral offset = 2(b/2). Equivalent full-scale wind speed = 35 knots. View looking upstream.

Table 1. Ship Geometry

	Full Scale LHA	**1/48th-scale model**
Flight deck length	820 ft	205.0 in
Flight deck width	118.1 ft	29.53 in
Nom. deck ht above waterline	64.5 ft	16.13 in
Landing Spot	Distance of nose-wheel mark from bow of ship (ft)	Location on Deck
1	46.5	Center
2	127.5	Port
4	232.5	Port
5	337.5	Port
6	442.5	Port
7	547.5	Port
8	697.5	Port
3	127.5	Starboard
3A	211.5	Starboard
9	697.5	Starboard

Table 2(a). Full Scale Aircraft Properties

	V-22 Osprey	**CH-46**
No. of rotors	2	2
No. blades per rotor	3	3
Rotor radius (in)	228.5	306.0
Blade tip chord (in)	22.00	18.75
Rotor solidity	0.1050	0.0585
Rotor RPM (100%)	397	264
Tip speed (ft/s)	792	705
Blade tip Reynolds number	9.26×10^6	7.03×10^6

Table 2(b). Approximate 1/48th-Scale Model Aircraft Properties

	Tilt-rotor	**Tandem-Rotor Helicopter**
No. of rotors	2	2
No. blades per rotor	3	3
Rotor radius (in)	4.687	6.311
Blade tip chord (in)	0.446	0.375
Rotor solidity	0.102	0.057
Rotor RPM (100%)	6355	4224
Tip speed (ft/s)	260	233
Blade tip Reynolds number	61,620	46,370

Table 3. Ship air-wake test conditions.

PIV Sheet Location[a]	V (ft/s)	Yaw (deg)
2	5.63	0,10
	11.25	0, 5, 10,15
	16.88	0, 10
	22.5	0, 5, 10,15
4	5.63	0,10
	11.25	0, 5, 10,15
	16.88	0, 10
	22.5	0, 5, 10,15
7	5.63	0,10
	11.25	0, 5, 10,15
	16.88	0, 10
	22.5	0, 5, 10,15
	28.13	0
	33.76	0
8	5.63	0,10
	11.25	0, 5, 10,15
	16.88	0, 10
	22.5	0, 5, 10,15
	28.13	0
	33.76	0

[a]PIV sheet was located 4.53 in downstream of the indicated landing spot